Springer

KSME

Journal of Mechanical Science and Technology 30 (12) (2016) 5715~5725
www.springerlink.com/content/1738-494x(Print)/1976-3824(Online)
DOI 10.1007/s12206-016-1142-1

Numerical study of an 870MW wall-fired boiler using De-NOx burners and an air staging system for low rank coal †

Min-Young Hwang[1,**], Seok-Gi Ahn[2,**], Ho-Chang Jang[3], Gyu-Bo Kim[4] and Chung-Hwan Jeon[2,*]

[1]*Research Institute of Industrial Science & Technology, Gwangyang 57801, Korea*
[2]*School of Mechanical Engineering, Pusan National University, Busan 609-735, Korea*
[3]*Korea South East Power Company, Jinju, Korea*
[4]*Pusan Clean Coal Center, Pusan National University, Busan 609-735, Korea*

(Manuscript Received February 14, 2016; Revised May 26, 2016; Accepted July 22, 2016)

Abstract

Pulverized coal-fired boilers have been used for power generation in Korea for decades. Recently, an 870-MW wall-fired boiler with De-NO_x [TM] burners and an air staging system was constructed for use with low-rank coal. The results of a full-scale simulation of its combustion characteristics agreed well with measurements obtained under normal operating conditions for temperature, unburned carbon, and nitric oxide. Contrasting trends in unburned carbon and NO_x emissions were observed, depending on the particle size and the location of the standby burner within the boiler. Combustion was also found to shift forward with small particle sizes and backward with large particle sizes. The results of a Thermo-mechanical analysis (TMA) indicated that the actual sticking temperature was lower than that suggested by the initial deformation temperature (ASTM) criteria. A logistic function was used to describe TMA shrinkage. Locations subject to high deposition potential were predicted with reference to soot-blowing phenomena.

Keywords: Coal combustion; De-NOx burners; NOx emissions; Simulation; Wall-fired boiler

1. Introduction

Pulverized coal-fired boilers (PCFBs) have been used to generate power in Korea for several decades, contributing 40 % of the total electricity produced. Recently, as the use of electric power has gradually increased as a result of industrial development, construction of new boilers has also steadily increased. However, PCFBs face technical challenges with respect to fuel flexibility and meeting environmental regulatory standards. The latter is particularly relevant given the strengthening of emissions regulations (including those for particulates, nitric oxide, and sulfur) in the country. From a technical perspective, the use of low-rank coal has been found to increase slagging and fouling, potentially leading to unexpected boiler shutdown. To address these issues, various de-NO_x technologies and slagging/fouling prediction tools have been developed and applied in the industry.

The NO_x forms produced in PCFBs are thermal NO_x, prompt NO_x, and fuel NO_x. Because most coal has a nitric component within the fuel, fuel NO_x is the major source of NO_x formation. During the coal combustion process, it is possible to reduce the formation of nitric oxide by two methods. Homogeneous reduction controls the reaction pathway in fuel lean/rich zones. In fuel-rich zones, the ammonia radicals that are formed from fuel nitrogen are mostly decomposed, leaving N_2. In excess-air zones, at common combustion system temperatures of more than 1000 °C, they are oxidized to form NO. Heterogeneous reduction is the reduction of residual char that has not yet undergone reaction. The very low level of NO formed from residual char is attributable to the reduction of NO on the surfaces of the coal particles. NO_x reduction can also be accomplished with air staging and fuel staging systems. Air and fuel staging techniques can be applied both in the boiler and at an individual burner. In the case of air or fuel staging in the furnace, there are clear, locally delimited zones with different stoichiometric conditions. When air or fuel staging is applied at a burner, the zone formation is affected by mixing processes.

The slagging and fouling that occur in a boiler originate in deposition phenomena. When deposited particles melt and form a sintered layer, the result is called slagging, whereas when ash particles form a layer through condensation at a relatively low temperature at a surface, it is called fouling. It is possible for these two phenomena to occur simultaneously or separately, depending on the temperature and surrounding environment.

*Corresponding author. Tel.: +82 51 510 3051, Fax.: +82 51 582 9818
E-mail address: chjeon@pusan.ac.kr
** Two authors contributed to this paper equally as the first author.
† Recommended by Associate Editor Jeong Park

Recently, the Korea South East Plant (KOSEP) constructed a wall-fired boiler with an 870-MW capacity that uses a De-NO_x burner and an air staging system and is intended for use with low-rank coal (5200 kcal/kg) rather than typical design coal (6080 kcal/kg). This is the first such boiler of this scale and type in Korea, and the use of a De-NO_x burner is also a first. Because this is new technology, it is important to obtain a better understanding of the combustion phenomena that occur within this boiler.

In this study, we used Computational fluid dynamics (CFD) to perform a simulation of the KOSEP 870-MW wall-fired boiler. The simulation included modeling of a De-NO_x burner and an air staging system. CFD models have been widely used to predict boiler performance [1-4]. Experiments on real-world large-scale systems involve very high utility costs and related safety problems; prediction through CFD has the advantage of providing detailed analyses of boilers without incurring significant expenses. Additionally, relevant phenomena were measured under the normal operating conditions of the boiler, and the measurements were then compared with the simulation results. The combustion mechanism of the De-NO_x burner was explored to identify possibilities for reducing NO_x emissions. Finally, the study examined the effects of standby burners and particle sizes, and explored the boiler's deposition potential.

2. Numerical modeling

2.1 Fuel properties

Studying solid fuel combustion requires that various experimental parameters (such as material properties and kinetics) be studied for each chemical reaction. Table 1 lists the properties of the KPU coal selected for the experiment. This coal type has properties similar to those of coal used in new low-rank coal boilers. Heat values were obtained using a differential scanning calorimeter. For several decades, the heating value of design coal has been 6080 kcal/kg; however, units 5 and 6 at the Young-Heung power plant use low-rank coal, with a heating value of 5200 kcal/kg. Proximate analysis was performed using a thermogravimetric analyzer (TA instrument SDT Q600), and ultimate analysis was performed using an element analyzer (LECO Tru-spec).

A particle size range of 45-150 μm is typically used for PCFBs, depending on the boiler geometry, coal reactivity, operating conditions, and experience of the boiler operator. For purposes of simulation, the Rosin-Rammler distribution provides realistic particle variations but also requires significant computational time. A uniform particle size was therefore used in this study. The selected demonstration particle had a 60-100 μm diameter distribution, while the measured mean diameter of the ash sample was determined to be 75 μm.

Slagging and fouling are major issues for low-rank coal combustion. To predict the deposition probability, the ash components and melting temperature were analyzed using American Society of Testing and Materials (ASTM) criteria.

Table 1. Properties of KPU coal.

Proximate analysis (% by mass, as received)	
Moisture	17.03
Volatile matter	39.77
Ash	6.65
Fixed carbon	36.55
Ultimate analysis (% by mass, daf basis)	
C	76.68
H	5.50
O	16.34
N	1.36
S	0.12
Ash composition (%)	
SiO_2	46.36
Al_2O_3	14.59
Fe_2O_3	6.18
CaO	5.16
MgO	1.72
Na_2O	5.97
K_2O	1.45
SO_2	0.86
TiO_2	5.48
Other	13.44
B/A ratio	0.308
Heating value (kcal/kg)	5190
IDT (K)	1419
ST (K)	1437
HT (K)	1464
FT (K)	1514

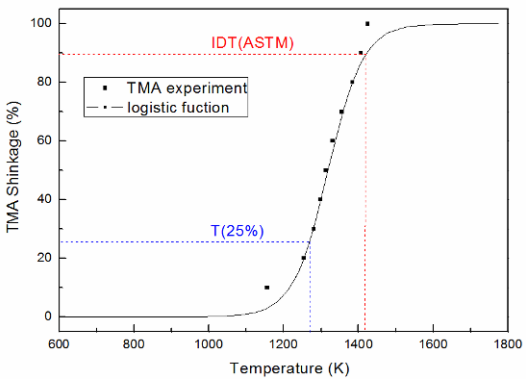

Fig. 1. TMA analysis results for KPU coal and mathematical fitting with logistic function, where, f(T) = α/[1+exp(a+bT)], α = 2.92, a = 22.308 and b = -0.02133.

The high-temperature area within the boiler was between 1500-1600 K, and the Fluid temperature (FT) was also within this range. Hence, it is expected that ash particles would be deposited on the tube surface. For the purpose of a more accurate melting temperature analysis, Thermo-mechanical analysis (TMA), an advanced experimental technique for coal ash slag [5], was performed. Fig. 1 shows the TMA results for KPU coal and the regression model fitted to the results. The temperature corresponding to TMA shrinkage of 25 % was known from the initial deformation, and the ASTM test results

showed it to be significantly lower than the Initial deformation temperature (IDT). At the IDT position, ash particles had melted completely. This means that the actual deformation temperature at which a particle becomes sticky is lower than the ASTM IDT value and thus the superheaters would be exposed to deposition problems. To identify the soot-blowing position, the melting behavior was analyzed using a logistic function in the simulation.

2.2 Particle dynamics model

Extensive kinetic studies have been conducted on coal reaction processes, which depend on temperature, environment, and coal rank. In this study, we used CFD parameters for devolatilization and apparent kinetics for char combustion; CFD parameters have been widely used and are referenced in many coal combustion simulation studies. Fluent 14.5 was used for the CFD process. This program allows various combustion models and source term options.

The Re-Normalisation Group (RNG) k-e turbulence model was used to account for swirling flow, and the P-1 model was used to account for radiative heat transfer effects, with an emissivity of 0.9 used for wall slag [6]. These models provide good approximate solutions for a full-scale boiler simulation without requiring excessive computation time. Detailed equations for mass, momentum, energy, and species transport are provided by Ma et al. [7]. To illustrate coal flow and combustion, a Dispersed phase model (DPM) was used. If the dispersed second phase occupies a low volume fraction (lower than 10 % of the total volume), the Euler-Lagrange approach can be considered an acceptable method. The dispersed phase is solved by tracking a large number of coal particles and allows for exchange of momentum, mass, and energy within the fluid phase.

2.3 Boiler geometry and De-NOx burner

Fig. 2 shows the three-dimensional (3D) geometry of the 870-MW pulverized coal boiler constructed by KOSEP in Korea in 2014. The real-scale simulator was developed with 2500000 cells. The burner zone is made up of three levels: Bottom (C, E), middle (A, B), and top (D, F). Each burner incorporates six multi-cylinder-shaped burners that face each other on the same level. Thus, the boiler has a total of 42 burners. The De-NO_x burner has four inlet ports, for Primary air (PA), Secondary air (SA), Tertiary air (TA), and Quaternary air (QA). The coal is carried by PA at 330 K, and there is a Flame-stabilizing ring (FSR) on the PA flow nozzle that allows locally fuel-rich/lean conditions to be created by controlling the surface in contact with the oxidizer. Hot air (SA, TA, and QA at 600 K) is connected with a wind box and controlled by a damper. Both TA and QA consist of swirling flow (45° angle), and each burner has an irregular swirl direction (clockwise/counter-clockwise, respectively), which allows mixing of the fuel and oxidizer within the volatile combustion area. A

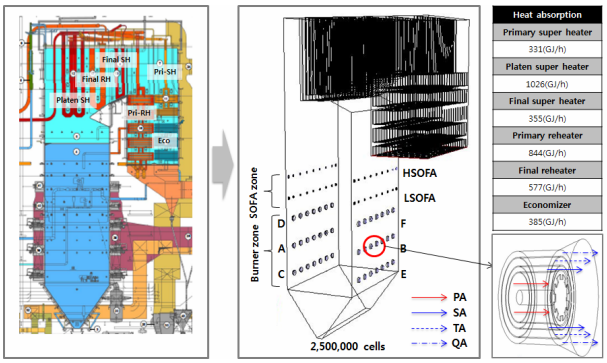

Fig. 2. Geometry of 870-MW wall-fired boiler (left), shape of De-NO_x™ burner (middle) and heat absorption values for superheater (right); PA = primary air and coal, SA = secondary air, TA = tertiary air, QA = quaternary air.

simplified geometry was considered for the burner in this calculation. While the shapes of the pipeline and swirl vane of each burner were not considered, the effective area of the nozzle tip was considered to set the boundary condition that would ensure the injection of coal and air from each surface. The swirls of tertiary air and quaternary air were considered using the normal vector and tangential vector at the nozzle surface. The Separated over-fire air (SOFA) zone is located at two levels (LSOFA, HSOFA) and also has swirl flow with an irregular direction. This SOFA system plays a role in air staging to reduce NO_x generation within the combustion area.

The heat sink/source dynamics of the following heat exchanger areas were modeled in this study: platen superheaters, final reheater and superheater, primary reheater, and economizer. The heat exchanger was actually designed as a bundle of circular tubes with a small diameter and a large heat transfer surface. However, it was impossible to consider the actual tube geometry because of the cell size, mesh problems, and significant increase in calculation time that this would have involved. The bundle of tubes was therefore simplified, and the heat transfer coefficient was recalculated for each heat consumption area based on the heat absorption data of each heat exchanger. Boundary conditions were calculated from real operational data and are listed in Table 2. The results of the real scale test at 870-MW performance are also provided.

2.4 Coal combustion model

Coal particles undergo very complex transformation processes during combustion, and no perfect illustration of both coal combustion and ash formation can be obtained; assumptions and simplifications are required. Fig. 3 illustrates the complex transformation behavior of coal particles and a simplified mechanism for full-scale simulation. Coal particles first release water vapor and then volatile matter as the temperature increases. Volatile and char burning then occur at contact locations with oxygen. Devolatilization and char combustion are slower reactions than evaporation and volatile burning. The reaction kinetics of these two processes are therefore impor-

Table 2. Operating conditions and measured values at 870-MW performance.

Supply conditions (Ton/h)			
	Coal	PA	SA + TA + QA
A burner	73.4	131.4	319.3
B burner	74.3	131.1	319.6
C burner	73.7	131	320.4
D burner	73.7	133.6	320.3
E burner	73.5	129.5	318.8
F burner	0	0	92.22
Total	368.6	656.6	1690.6

	SOFA
LSOFA (front wall)	199.02
LSOFA (rear wall)	174.53
HSOFA (front wall)	257.7
HSOFA (rear wall)	257.6
Total	888.85

Measured value before Selective catalytic reduction (SCR) at 870-MW performance	
O_2(%)	2.5 ± 0.5 %
UBC (%)	3 ± 1 %
NO_x(ppm)	102.5 ± 10 ppm
Outlet temperature (K)	630 ± 3 K

Measured temperature within boiler at 870-MW performance	
Nose temperature (K)	1527
F.E. temperature (K)	1322

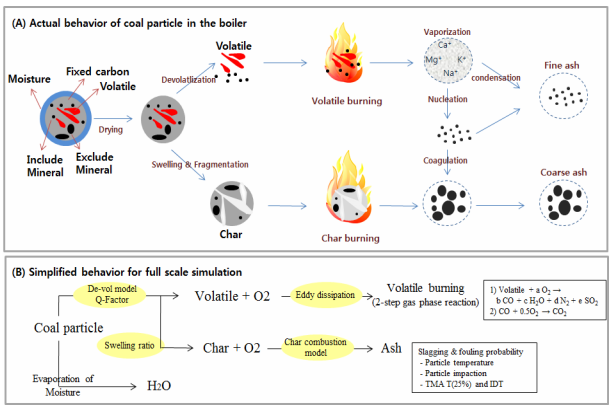

Fig. 3. Coal combustion behavior in the boiler and simplification for full-scale simulation.

tant in controlling the overall burning time.

Devolatilization: When coal is heated to a sufficiently high temperature, it begins to decompose, producing tars, gases, and volatiles. These processes depend not only on the temperature but also on the molecular structure of the coal. Many researchers have tried to obtain generalizations of complicated devolatilization processes and have produced various useful simplified models for practical application. The most basic mathematical devolatilization model assumes that raw coal is only a reactive material in the coal particle and calculates the generation rate experimentally. Single [8] and two-competing rates [9] are representative first-order reaction rates. Another class of devolatilization model is the network model, which reflects the chemical nature of pyrolysis behavior. FG-DVC [10], FLASHCHAIN [11], and CPD [12] have been used successfully to describe the influence of the chemical features of coal on devolatilization behavior under various burning conditions. In this study, we used a CFD model for simulation, with the following coefficients: sig+1 = 4.97, MW = 367.5, M_del = 39.7, p0 = 0.51, and c0 = 0.0538. These values were derived using the C^{13} NMR parameter calculator program developed by Fletcher et al. [12]. The high volatile yield (Q-factor) was taken from Jensen and Mitchell [13].

Char combustion: Char, which is the solid residue remaining after pyrolysis, has various textures (hollow, network, skeleton, balloon, etc.). These shapes depend on the maceral contents of the parent coal and on the devolatilization conditions. The reaction rates of such porous particles are related to structural factors (particle diameter, porosity, specific surface area, pore diameter, etc.), as well as the intrinsic reactivity and diffusion of reactants to the particle surface [14]. There are three reaction regimes for the combustion of char particles, which depend on the temperature. In the low-temperature range, the chemical reaction is the limiting factor (Zone 1). In the mid-temperature range, the reaction rate is controlled by both chemical factors and pore diffusion (Zone 2). In the high-temperature range, diffusion of oxygen to the particle surface limits the reaction rate of char combustion (Zone 3).

The intrinsic model is well known to describe variations in the char reaction rate but requires advanced empirical values for pore development. For the purpose of the full-scale simulation, considering that the char combustion environment in the boiler was predominantly within Zone 3, we used apparent kinetics instead of intrinsic kinetics to calculate the char combustion. The model used for the char combustion simulation in this study was the kinetic/diffusion surface reaction rate, as elaborated by Baum and Street [15] and Field [16]. This model assumes that the surface reaction rate includes the effects of both bulk diffusion and chemical reaction. The n^{th}-order global reaction used to determine the char oxidation rate is given as follows:

$$q_p = -\pi d_p^2 \frac{\rho R T_\infty Y_{ox}}{M_{w,ox}} k_c P_{gas,s}^n \tag{1}$$

where q_p is the reaction rate (kg/s) and d_p is the particle size. Because the particle size in the PCFB is 75-100 μm, a single film model is appropriate for reaction modeling. The boundary layer diffusion is given as follows:

$$A_p h_d \left(P_{gas,\infty} - P_{gas,s} \right) = A_p k_c P_{gas,s}^n$$

and

$$k_c = A_c \exp\left(-\frac{E}{RT_p} \right) \tag{2}$$

where for the simple equation, the reaction order n was considered to be 1. This is an important assumption when using the kinetic diffusion model provided in the Fluent char combustion model. Eq. (2) can thus be rewritten as follows:

$$q_p = -\pi d_p^2 \frac{\rho R T_\infty Y_{ox}}{M_{w,ox}} \frac{h_d k}{(h_d + k)} \tag{3}$$

and q_p and h_d are given by Eqs. (4) and (5):

$$q_p = \frac{\Delta m}{\Delta t} \tag{4}$$

$$h_d = C_1 \frac{\left[(T_p + T_\infty / 2\right]}{d_p}. \tag{5}$$

Finally, the kinetics of char oxidation can be expressed as follows:

$$R_k = \left[\frac{h_d k}{(h_d + k)}\right] = \left(-\frac{q_p}{\pi d_p^2 \frac{\rho R T_\infty Y_{ox}}{M_{w,ox}}}\right) \tag{6}$$

where the left-side term is a function of the particle temperature and the right-side term is a function of q_p at a given particle temperature and particle pressure of oxygen. At low temperatures, k_c is greater than h_d. Thus, k_c is a limiting rate. In contrast, at a high temperature, h_d is greater than k_c and h_d is the limiting rate. The transition temperature between k_c and h_d is dependent on the heterogeneous reactivity of the char. In this study, a Wire mesh reactor (WMR) was used to determine the char oxidation rate. The WMR, which has been validated by numerous investigators, was designed and constructed to investigate the combustion and gasification kinetics of coal particles. Details concerning this apparatus are given elsewhere [17-19]. A comparison of the calculated and experimental reaction rates for KPU coal is shown in Fig. 4. The calculated kinetic diffusion rate matches the experimental results reasonable well for the following values used: $C_1 = 4 \times 10^{-12}$ KJ/kmol, A = 1.07×10^{-2} KJ/kmol, and E = 6.92×10^4 KJ/kmol.

Volatile combustion: The eddy dissipation model was used for the gas-phase reaction of volatile matter released from the coal. Based on the work of Magnussen and Hjertager [20], this model assumes that overall gas-phase reactions are controlled by turbulent mixing. In general, the Arrhenius kinetic rate at the ignition spot is greater than the eddy dissipation rate. This means that the reaction rate of the gas phase is governed by turbulence. Due to high atmospheric temperatures, the combustion of volatile matter is based on a fast-burning process in a PCFB. In this case, the Arrhenius rate model can be ignored to reduce the computation time.

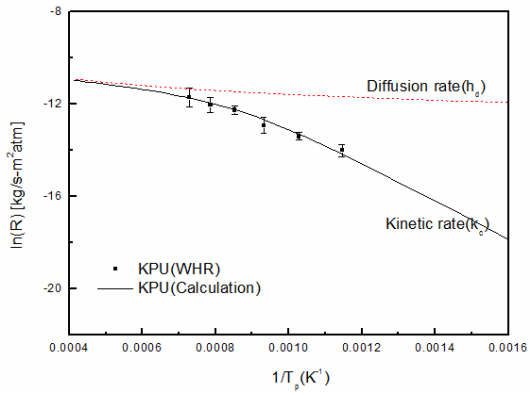

Fig. 4. Comparison of calculated and experimental char oxidation rates for KPU coal.

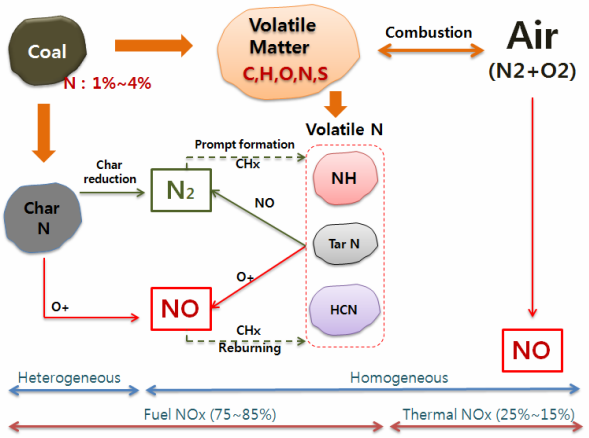

Fig. 5. NO_x formation mechanism within the pulverized coal boiler.

2.5 NOx model

The nitrogen oxides that are formed in the PCFB are derived from two sources. The first is oxidation of fuel nitrogen, referred to as fuel NO_x, and the second is oxidation of nitrogen in the air, referred to as thermal NO_x. It is well known that fuel NO_x makes up 75-85 % of the nitrogen oxides in PCFBs, while thermal NO_x makes up 15-25 % of this total [20]. NO, NO_2, and N_2O are also formed during pyrolysis, but in a PCFB environment, more than 90 % of the NO_x occurs in the form of NO; for this reason, only the latter was considered in this study. Most experimental studies on coal pyrolysis report that coal nitrogen is released from both volatiles and residual char. There are multiple-step reactions that occur as volatile nitrogen reacts with oxygen before finally forming NO_x, in addition to char nitrogen participating in heterogeneous surface reactions that lead to NO formation. However, details of the chemical reactions can be avoided to reduce the calculation time when dealing with a full-scale problem. For this reason, only global reactions and major mechanisms were considered and are shown in Fig. 5. To reduce NO conversion, fuel-rich regions (i.e., a reducing environment) should be formed in the combustion area.

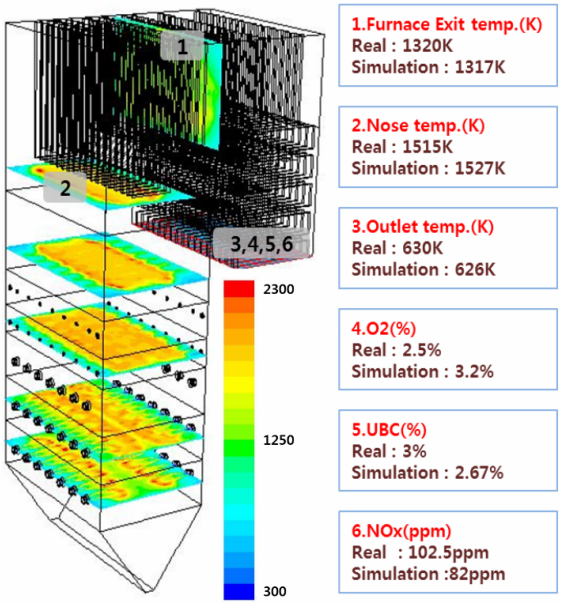

Fig. 6. Comparison of simulated and measured results at different positions.

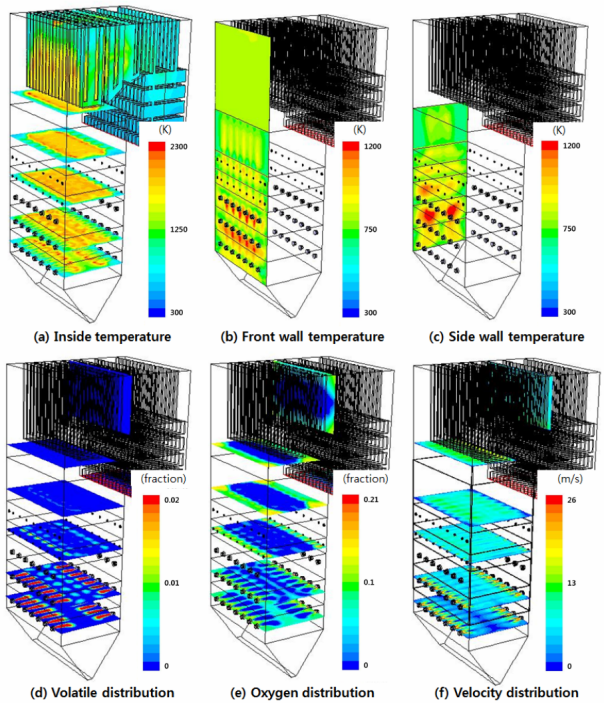

Fig. 7. Contours of simulated results under 870 MW operating conditions.

3. Results and discussion

The coal combustion simulation required that values be assigned to many input parameters, such as the boundary conditions for each burner, the coal properties, and the kinetic values for each reaction. The simulation was also based on assumptions related to numerical equations and calculations and therefore was not a perfect representation of heterogeneous coal combustion processes. Ideally, at least one simulation case should be matched with real test results before changing parameters in the boiler. Table 2 lists the supply conditions and measured values that apply under normal operating conditions. The simulation was performed under the same conditions, and the results were compared with the measured values. Fig. 6 shows a comparison of the predicted temperature field within the boiler and the real-case results for the same position. Locations 1 and 2 are significant and are referred to as the nose temperature and furnace exit temperature regions, respectively. The nose temperature region is the first heat exchange region between the flue gas and the superheater. This zone has high potential for slagging due to high temperatures. The furnace exit temperature region is located in the middle of the heat exchanger area and provides information on whether post combustion has occurred. The real values of these points were measured using the Zolo-BOSS (Boiler optimization spectroscopy sensor) system. The simulation results showed good agreement with the real values. The simulated and measured temperature values agreed well, and reasonable agreement was also obtained for oxygen and Unburned carbon (UBC). However, the measured NO_x values were lower than that indicated by the simulation, which could be due to a local leak, such as one at the bottom ash port in the real boiler. Entrained air can also contribute to NO_x generation, increasing fuel NO_x by influencing the fuel-rich region with volatile combustion in the burner zone.

3.1 Normal conditions

Fig. 7 shows contours of simulation results at 870-MW-performance operating conditions. Fig. 7(a) shows the temperature distribution within the boiler. Hot gases were generated by the burner and merged along the flue gas direction. The hot gases display a square, planar shape after the SOFA area and become narrow with increasing velocity at the nose location. Both concentrated hot flue gases and increased velocity increase the convective heat transfer of the platen superheater. Figs. 7(b) and (c) show the front- and side-wall temperatures, respectively. Both the middle (A, B) and top-level (D, F) burner walls were exposed to hot gas damage, while the bottom-level (C, E) burner wall was within a safe temperature range. The middle-side wall also was a high temperature area, because of the middle-level burners being surrounded by top and bottom burners. Figs. 7(d) and (e) show the concentrations of volatiles and oxygen, respectively. The greatest release of volatiles from the coal occurred near the burner, where oxygen consumption was also significant. Central locations therefore have very limited oxygen concentrations because most of the supplied air is consumed near the burner, which contributes to a reduction in fuel NO_x by providing a reducing environment.

Fig. 8 shows contours in horizontal planes at burner locations A and B. Volatiles were rapidly released near the burner,

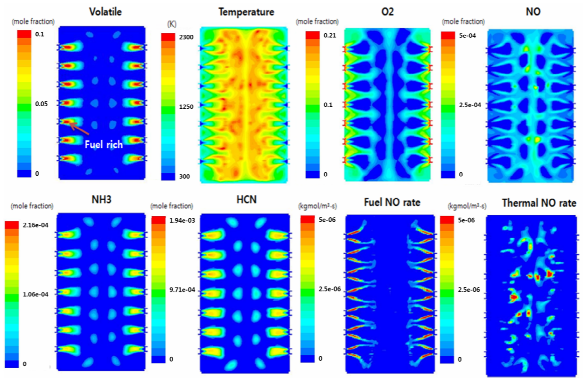

Fig. 8. Contours of simulation results on the horizontal plane of middle (A, B) burners.

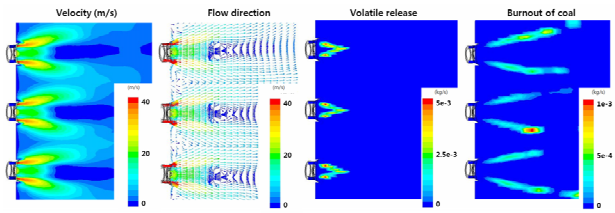

Fig. 9. Contours of velocity, flow direction, volatile release, and burnout of coal on the horizontal plane of the middle burner.

and a flame was formed where contact occurred between the volatiles and secondary air. Both NH_3 and HCN were released with the volatiles and reacted with oxygen. The figure clearly shows that fuel NO_x formed to a large degree where adequate temperature and oxygen concentrations were present. In addition, thermal NO_x was formed from hot spots where flames overlapped. The figure illustrates that fuel NO_x is the dominant contributor to NO_x emissions.

Fig. 9 shows contours of the velocity, flow direction, volatile release area, and burnout of coal near the burner. The TA and QA nozzle velocities were larger than the PA velocity and exhibited a swirl effect, which increased mixing between the fuel and the air. This difference also created a recirculation zone within the volatile release area.

Fig. 10 illustrates the combustion mechanism of the De-NO_x burner and summarizes the results shown in Figs. 8 and 9. Pulverized coal and primary air first form a concentrated fuel flow due to the FSR. This plays a role in concentrating particles within the devolatilization zone. Subsequently, velocity differences create recirculation flows within the volatile area, driving the formation of volatile-rich zones and particle movement. Volatile combustion occurs at the boundary of the volatile zone where secondary air (SA, TA, QA) has sufficient oxygen, a relatively high temperature (PA = 330 K; SA, TA, QA = 610 K), and swirl flow (TA, QA). After the pre-volatile combustion zone, the char particles dispersed by internal recirculation flow move into the flame area, and char combustion proceeds. NO_x emission could be effectively controlled through this combustion mechanism. Fig. 8 shows the temperature of the burner and distribution of chemical species. At

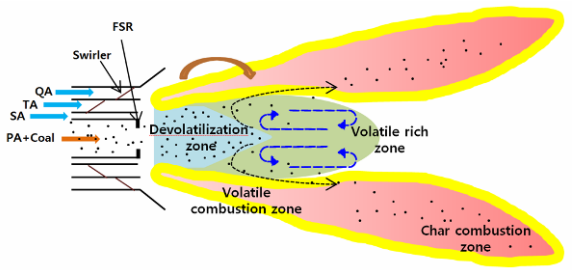

Fig. 10. Combustion mechanism of De-NO_x™ burner. FSR = flame stabilizer ring, PA = primary air, SA = secondary air, TA = tertiary air, QA = quaternary air burner.

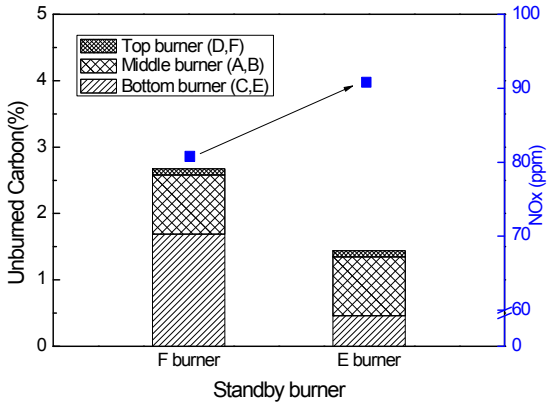

Fig. 11. Simulated unburned carbon and NO_x values before SCR under E, F burner standby conditions.

the end of the burner nozzle tip, volatile concentration is distributed, and on the boundary surface, which is in contact with the secondary air, volatile combustion occurs. Accordingly, fuel NO_x creation is reduced in the fuel rich zone where volatile concentration is high and oxygen concentration is low, but fuel NO_x creation is active in the volatile combustion zone. We can conclude that the De-NO_x burner can be used to effectively control fuel-rich/lean regions and thereby reduce NO_x emissions.

3.2 Effect of standby burner

Not every burner operates under normal conditions. To prepare for an emergency situation, at least one layer (the F or E burner) was considered to be in standby mode. Fig. 11 illustrates the simulated Unburned coal (UBC) and NO_x values under standby conditions for the E and F burners, respectively. First, there is a difference in UBC between the burners, even though each burner has an equal load (coal and air flow). These results can be explained in terms of the particle pathway and oxygen distribution in the boiler. The fuel supplied to a bottom burner moves toward the center of the boiler; on the other hand, fuel supplied to middle or top burners cannot penetrate to the center. This is due to the total mass flow increasing, with the result that the expanded gas volume develops a strong upward momentum. This produces different particle

pathways between burners. Consequently, bottom-burner (C and E) particles are influenced to a relatively small degree by upper momentum and therefore pass the low-oxygen area (the center of the boiler), creating large quantities of UBC, even though bottom-level fuel has a higher residence time than fuel at upper levels. Accordingly, Fig. 11 shows that when burner F is the standby burner, the UBC increases, compared to the case when burner E is the standby burner. Based on the UBC at each burner position, the UBC value was high for the coal injected from the bottom burner (C, E), and the standby burner position had a clear effect on combustibility. For NO_x emission, the result is opposite to that of the UBC. In other words, when burner F is the standby burner, NO_x emission is low. The NO_x result can be explained by the relationship between NO_x and oxygen. For the fuel NO_x generated by coal burning, creation and reduction mechanism occurs in the volatile combustion stage depending on the oxidizing/reducing environment. Air staging for NO_x reduction creates a reducing environment in the burner zone, which reduces NO_x and causes the burnout of the unburned carbon in the SOFA zone. The longer the fuel rich zone, which ranges from air staging burner to SOFA zone, the greater the effect on NO_x reduction. When burner F is the standby burner, it will have more time than burner E (standby burner) until it is exposed to staged air, thereby reducing NO_x emission. Fig. 12(a) clearly shows this effect and also indicates that the NO_x level is low when burner F is the standby burner in the initial burner zone.

Fig. 12 shows the average NO_x, temperature, and oxygen variation in the boiler. There are lower oxygen concentrations with the F burner in standby than with the E burner in standby. This is due to use of the E burner (with the F burner on standby), leading to a greater consumption of oxygen by volatile combustion in the burner zone. Low oxygen concentrations create a more fuel-rich region on the burner zone, leading to a reduction in the generation of fuel NO_x.

3.3 Effect of particle size

The power plant typically uses a 75-μm particle size for PCFBs; however, the combustion regime could be shifted forward or backward by the coal quality. Changes in both the nose temperature and furnace exit temperature lead to irregular efficiency. These, therefore, need to be well controlled for continuous power generation. Particle size is one of the operating conditions that can be varied to control coal combustion and mitigate coal quality problems. Fig. 13 compares the temperature, NO_x, and UBC results as a function of the particle size criterion.

Fig. 14 shows the particle temperature variations for each condition. The overall trends show that NO_x emissions decrease with increasing particle size, while UBC increases. The nose temperature decreases with increasing particle size, but the opposite applies to the furnace exit temperature. These results indicate that the combustion area changes with particle size. When the supplied particle size is smaller, the combustion is shifted forward because of the increased particle surface area, which results in a higher particle temperature, more rapid completion of combustion, and possible reductions in UBC. However, increased particle temperatures greatly increase NO_x, creating a hot spot (with a temperature of more than 1800 K) that significantly accelerates thermal NO_x formation. When the supplied particle size is larger, combustion

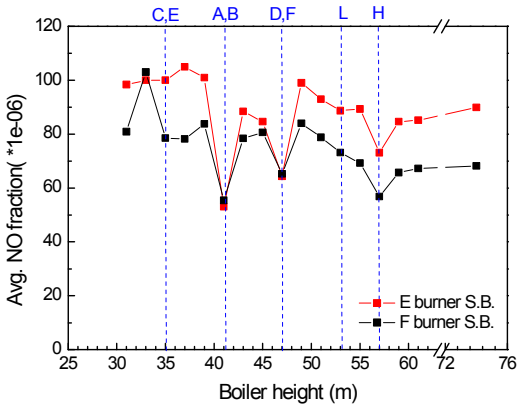

(a)

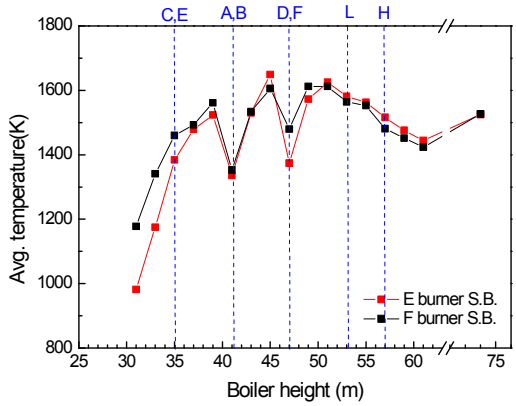

(b)

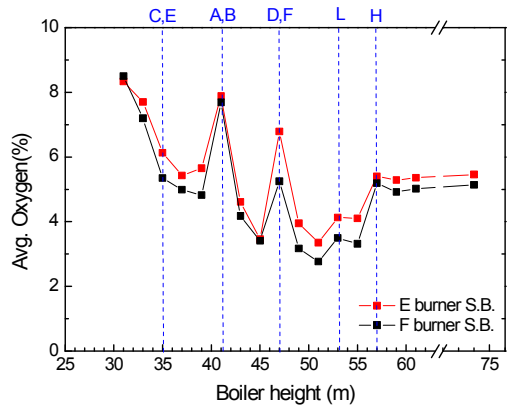

(c)

Fig. 12. Average NO_x, temperature and oxygen variations with boiler height under E, F standby burner conditions. A,B,C,D,E,F = burner locations, L = LSOFA, H = HSOFA: (a) Average NO fraction; (b) average temperature; (c) average oxygen.

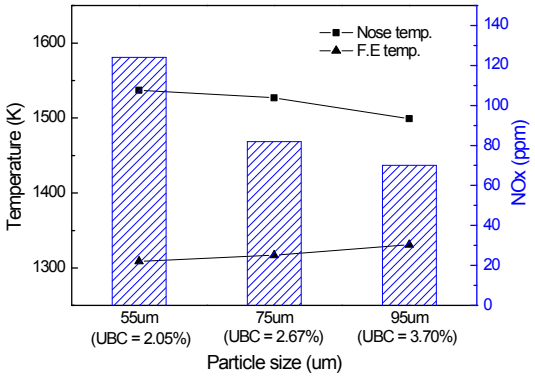

Fig. 13. Simulated temperatures, NO_x and UBC results as a function of particle size.

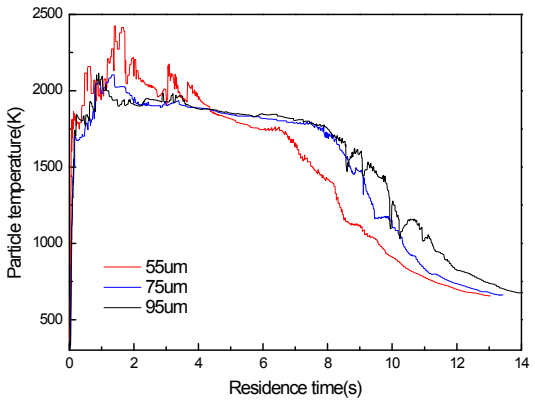

Fig. 14. Particle temperature variations as a function of particle size (C burner particle data).

is shifted backward because of the decreased particle surface area, which leads to an increase in UBC. However, NO_x decreases slightly with decreasing particle temperature, and the reduced amount is smaller than the 55-μm result, as a result of thermal NO_x not appearing to be a major source.

3.4 Deposition potential

The deposition of molten ash particles is one of the challenging issues in PCFB operation when low-rank coal is used. There has been extensive research to model ash transformation processes using mathematical functions, but it is impossible for these to provide perfect representations of slagging and fouling, taking into account ash components, turbulence effects, size distribution, the combustion environment, and shedding phenomena. Such models also require a large quantity of experimental data, additional calculation time, and advanced programming skills to define user functions. More accurate modeling is needed; however, there is also a need for simple modeling, using less demanding methods, to determine the deposition potential using full-scale simulation, even if this does not include a detailed description of the deposition mechanisms.

The melting temperature is a key factor in the irregular

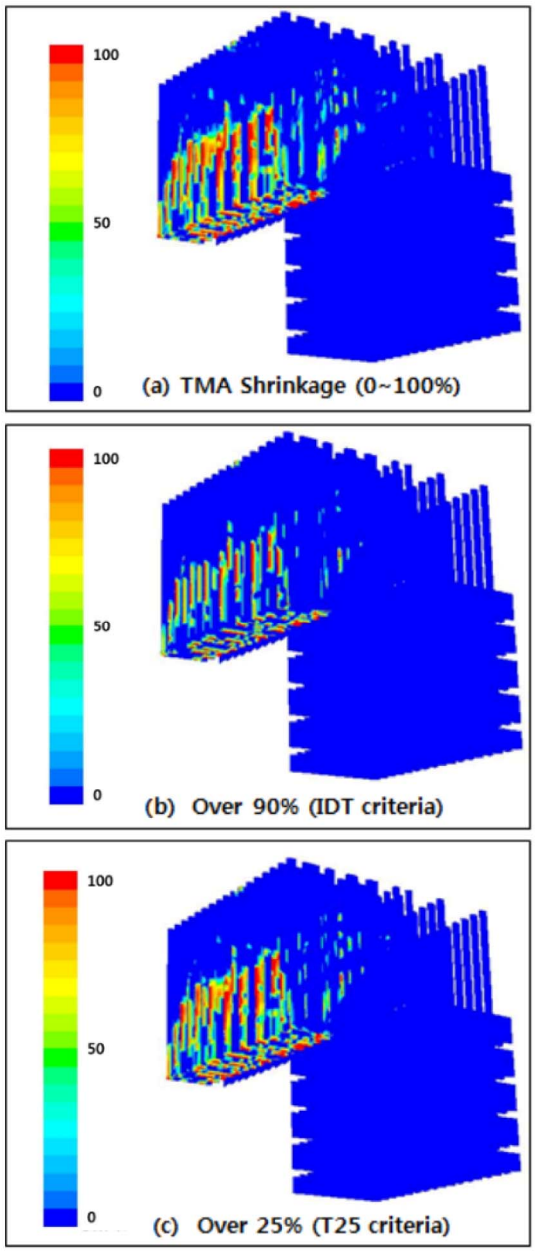

Fig. 15. Direct application of TMA results using logistic functions: (a) Contours of TMA shrinkage; (b) contours of shrinkage at 90 % threshold (IDT criteria); (c) contours of shrinkage at 25 % threshold (T25 criterion).

characteristics of ash transformation. To obtain a more accurate value for the melting temperature, we examined the TMA test and derived a logistic function for the TMA shrinkage value. The logistic function for KPU coal can be expressed as follows:

$$\text{TMA Shrinkage}(\%) = 2.92 / \left[1 + \exp\left(22.308 - 0.02133 T_p\right)\right]. \quad (7)$$

The Fluent code accommodates User-defined functions

(UDFs), and Eq. (7) can be used as a UDF. Fig. 15 shows contours of the TMA shrinkage results. Fig. 15(a) shows the particle impact location and TMA shrinkage on a spectrum from 0-100 %, based on the particle temperature at the particle impact position. The IDT point is considered to be the sticking temperature, according to ASTM criteria, and the TMA criteria refer to a shrinkage value of 25 % (T25) for the IDT. The ASTM IDT point was matched with a 90 % shrinkage value in the TMA results. Fig. 15(b) illustrates this threshold, where particles are considered to have deposition potential when IDT criteria are employed. Fig. 15(c) shows the 25 % threshold (T25 criterion). Given that T25 is a lower temperature than the IDT, the results show that this criterion results in greater deposition potential. The majority of the deposition potential is evident on the platen superheater zone. It was therefore concluded that this zone is susceptible to an ash deposition problem and that soot blowing may be needed in the red zones in the figure. Using this method, TMA shrinkage results could be used for simple description purposes, and the deposition potential can be predicted using full-scale simulation.

4. Conclusions

To understand the combustion characteristics of an 870-MW wall-fired boiler, a simulation was conducted, and the results were matched with real-world measurements. Both standby burner conditions and the effects of particle size were simulated and analyzed. A TMA analysis was also performed to determine the actual sticking temperature and predict the deposition potential.

(1) The simulation results were validated under normal operating conditions and showed good agreement with real-world values with respect to temperature, NO_x, and UBC. The temperature and species (volatiles, oxygen, NH_3, HCN, and NO_x) fields were analyzed to obtain insights into understanding how combustion occurs within the boiler.

(2) Use of bottom-level burners (C, E) was shown to be useful in reducing NO_x by creating fuel-rich regions in the burner zone. However, the UBC increased because of particles passing through the centerline of the boiler. Conversely, use of top-level burners (D, F) led to reductions in the UBC but increases in NO_x. This counter-effect could be useful when using high-N-containing coal or low-combustion-quality coal.

(3) The effects of different particle sizes (55 μm, 75 μm, and 95 μm) were compared. The results indicate that smaller particles lead to forward shifts in combustion, increases in NO_x, and decreases in UBC, whereas larger particle sizes lead to backward shifts in combustion, decreases in NO_x, and increases in UBC). Particle size is therefore an effective tool for use in operational control of coal combustion.

(4) The TMA results show that the sticking temperature is lower than the IDT. A logistic function was derived to describe the TMA penetration results of the full-scale simulation. Locations exposed to high deposition potential were predicted for purposes of soot blowing.

Acknowledgment

This work was supported by the Korea Institute of Energy Research (KIER) (No.D6-2469) and the Korea Institute of Energy Technology Evaluation and Planning (KETEP) and the Ministry of Trade, Industry & Energy (MOTIE) (No. 20131010101830) of the Republic of Korea.

Nomenclature

q_p	: Reaction rate
d_p	: Particle size
ρ	: Density
R	: Gas-law constant
M_w	: Molecular weight
T	: Temperature on Celsius temperature scale
k_c	: Kinetic rate
A_p	: Surface area
H_d	: Diffusion rate
Y_{ox}	: Oxidant mass fraction
P_{ox}	: Partial pressure of oxidant species in the gas surrounding the combusting particle
E	: Activation energy
A_c	: Pre-exponential factor
h_d	: Diffusion rate coefficient
m	: Mass
t	: Time
R_k	: Kinetics of char oxidation
T_p	: Particle temperature

References

[1] A. Weiguo and M. K. Jhon, Simulation of coal ash particle deposition experiments, *Energ. Fuel* (2011) 708-718.

[2] L. Ma, J. M. Jones, M. Pourkashanian and A. Williams, Modelling the combustion of pulverized biomass in an industrial combustion test furnace, *Fuel,* 86 (2007) 1959-1965.

[3] A. Bosoaga, N. Panoiu, L. Mihaescu, R. I. Backreedy, L. Ma, M. Pourkashanian and A. Williams, The combustion of pulverized low grade lignite, *Fuel,* 85 (2006) 1591-1598.

[4] Y. M. Sung, C. H. Choi, C. E. Moon, S. Y. Eom, J. J. Lee, B. D. Kim, G. M. Choi and D. J. Kim, Nitric oxide emissions and combustion performance of nontraditional ring-fired boilers with furnace geometries, *Journal of Mechanical Science and Technology*, 29 (8) (2015) 3489-3499.

[5] R. P. Gupta, T. F. Wall and L. Baxter, Impact of mineral impurities in solid fuel combustion, *Proc. Eng. Found. Conf. Miner. Matt. Fuel.* (1997) 155-169.

[6] R. I. Backreedy, L. M. Fletcher, J. M. Jones, L. Ma, M. Pourkashanian and A. Williams, Co-firing pulverized coal and biomass: a modeling approach, *Proc. Combust. Inst.,* 30 (2005) 2955-2964.

[7] L. Ma, M. Gharebaghi, R. Porter, M. Pourkashanian, J. M. Jones and A. Williams, Modelling methods for co-fired pulverized fuel furnace, *Fuel,* 88 (2009) 2248-2249.

[8] D. W. Van Krevelen, C. Van Heerden and F. J. Huntgens, Physicochemical aspects of the pyrolysis of coal and related organic compounds, *Fuel,* 30 (1951) 253.
[9] H. Kobayashi, J. B. Howard and A. F. Salofim, Coal devolatilization at high temperatures, *Proc. Combust. Inst.,* 16 (1977) 411.
[10] P. R. Solomon, D. G. Humblem, R. M. Carangelo, M. A. Serio and G. V. Despande, General model of coal devolatilization, *Energ. Fuel,* 2 (1988) 405.
[11] S. Niksa and A. Kerstein, Flashchain theory for rapid coal devolatilization kinetics, 1. Formulation, *Energ. Fuel*, 5 (1991) 647.
[12] T. H. Fletcher, A. R. Kerstein, R. J. Pugmire, M. S. Solem and D. M. Grant, Chemical percolation model for devolatilization, 3. Direct use of ^{13}C NMR data to predict effects of coal type, *Energ. Fuel,* 6 (1992) 414.
[13] P. T. Jenson and R. E. Mitchell, *High-temperature char reactivity measurement in the Sandia laminar flow reactor*, Project No. 1323/87-16 (1993).
[14] I. Kuniyoshi, *Advanced pulverized coal injection technology and blast furnace operation*, Burlington: Elsevier (2000).
[15] M. M. Baum and P. J. Street, Predicting the combustion behavior of coal particles, *Combust. Sci. Tech.,* 3 (5) (1971) 231-343.
[16] M. A. Field, Rate of combustion of size-graded fraction of char from a low-rank coal between 1200 K-2000 K, *Combust. Flame,* 13 (1969) 237-252.
[17] R. G. Kim and C. H. Jeon, Intrinsic reaction kinetics of coal char combustion by direct measurement of ignition temperature, *Appl. Therm. Eng.,* 63 (2014) 565-576.
[18] R. G. Kim, C. W. Hwang and C. H. Jeon, Kinetics of coal char gasification with CO_2: Impact of internal/external diffusion at high temperature and elevated pressure, *Appl. Energ.,* 129 (2014) 299-307.
[19] M. Y. Hwang, S. M. Kim, G. B. Kim, B. H. Lee, J. H. Song, M. S. Park and C. H. Jeon, Simulation studies on direct ash recycling and reburning technology in a tangential fired 500 MW pulverized coal boiler, *Fuel,* 112 (2013) 78-87.
[20] B. F. Magnussen and B. H. Hjertager, On mathematical models of turbulent combustion with special emphasis on soot formation and combustion, *Proc. Combust. Inst.,* 16 (1977) 719-729.
[21] S. C. Hill and L. D. Smoot, Modeling of nitrogen oxides formation and destruction in combustion systems, *Prog. Energ. Combust.,* 26 (2000) 417-458.

Min-Young Hwang received his B.S. (2008), M.S. (2010), and Ph.D. (2015) degrees from Pusan National University. He is currently a Principal Research Engineer at the Research Institute of Industrial Science & Technology.

Seok-Gi Ahn received his B.S. (2013) and M.S. (2015) degrees from Pusan National University. He is currently Ph.D. course in the School of Mechanical Engineering at Pusan National University.

Ho-Chang Jang received his B.S. (1992) from Pukyong National University and M.S. (2014) degrees from Pusan National University. He is currently Senior Manager in Yeosu Division at Korea South-East Power Corporation.

Gyu-Bo Kim received his B.S. (2002) from Pukyong National University, Ph.D. (2008) degrees from Pusan National University. Dr. Kim is currently a Research Professor in the Pusan Clean Coal Center.

Chung-Hwan Jeon received his B.S. (1985), M.S. (1987), and Ph.D. (1994) degrees from Pusan National University. Dr. Jeon is currently a Professor in the School of Mechanical Engineering at Pusan National University and is currently serving as a Director of the Pusan Clean Coal Center.